
Transport of helium as an impurity and as a main ion in Alcator C-Mod*

**K. T. Liao, W. L. Rowan, I. O. Bespamyatnov, W. Horton, and
X.R. Fu**

*Institute of Fusion Studies, The University of Texas at Austin,
Austin, TX 78712*

*U.S. Transport Task Force Workshop
10-13 April, Annapolis, MD*

**Supported by USDoE
Awards DE-FG03-96ER54373 and DE-FC02-99-ER54512*

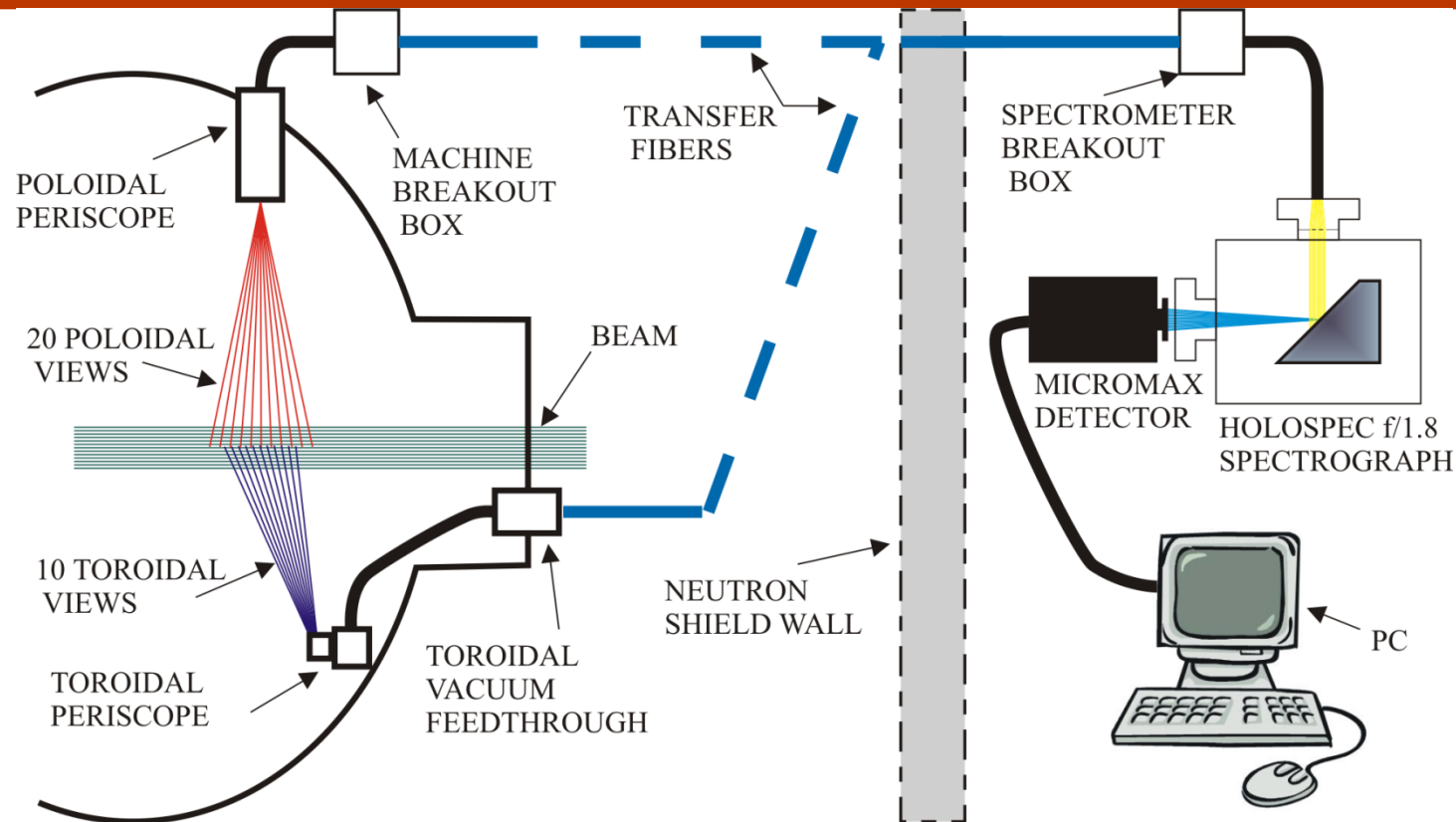
Summary

- ◆ Local density, temperature, and flow velocity measurements of helium in the Alcator C-Mod tokamak are provided by Charge Exchange Recombination Spectroscopy (CXRS).
- ◆ Measurements have been taken in L and H modes, and for helium as an impurity and helium as the main ion.
- ◆ Understanding helium impurity transport is important in ultimately controlling helium ash accumulation in a burning plasma experiment. Experiments on other tokamaks have shown that the transport coefficients depend heavily on the discharge regime and machine.
- ◆ The sensitivities of the logarithmic gradient to several plasma parameters are given, and compared to predictions of neoclassical theory and analytical treatment of drift wave turbulence.
- ◆ The helium measurements supplement a growing set of boron impurity measurements. These are used for light impurity transport studies.
- ◆ Local helium measurement is also needed for RF deposition experiments in (^3He minority) D plasmas for determination of the deposition mode. These results support turbulence measurements from the phase contrast imaging diagnostic.

Introduction

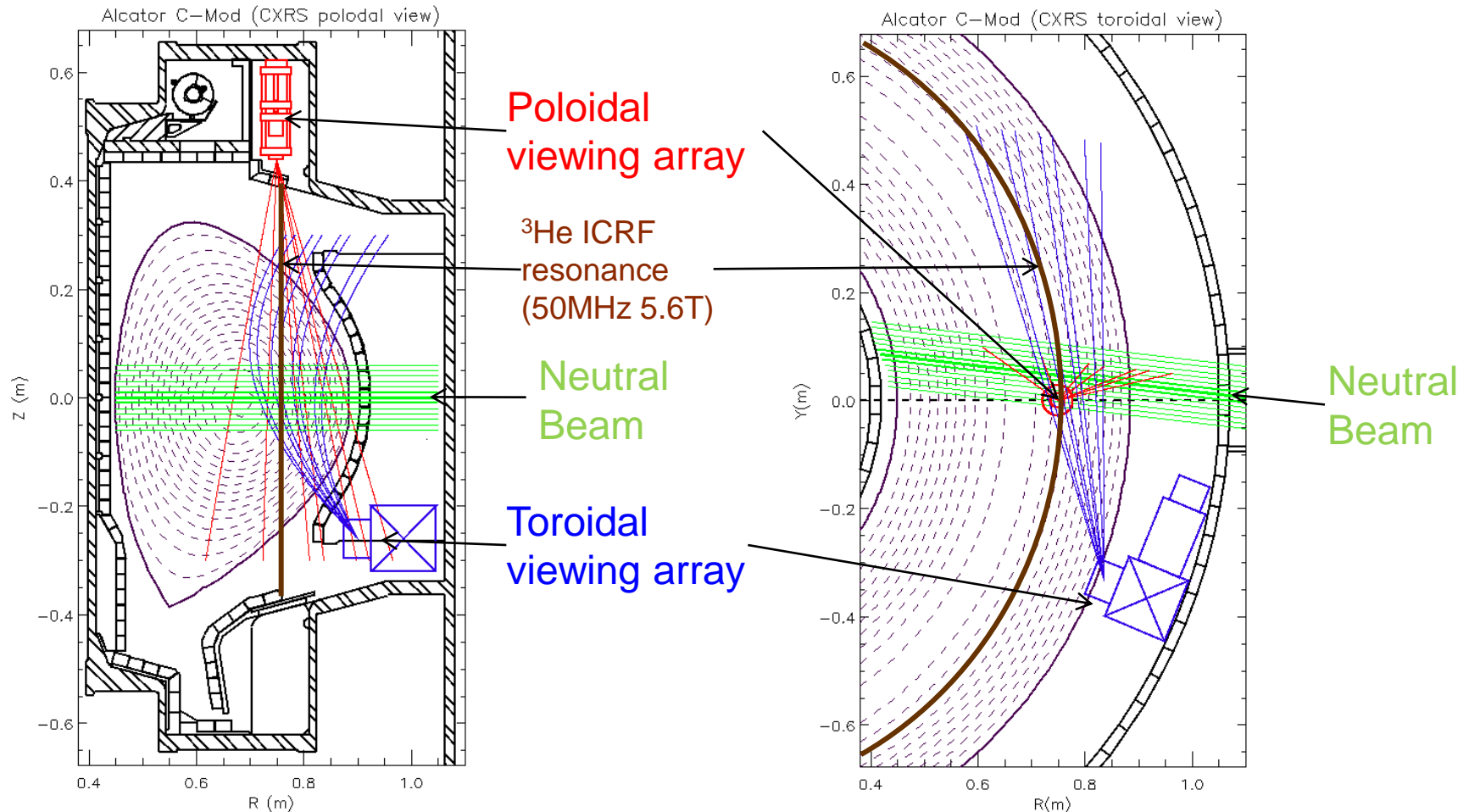
- ◆ Helium is an unavoidable impurity in a thermonuclear reactor as a product of the D-T reaction (among others). Understanding the transport of helium is essential to avoiding excessive accumulation of the impurity which will increase radiative losses and dilute the fuel.
- ◆ Experiments on other tokamaks have shown that the transport coefficients depends heavily on the discharge regime and machine. Unfortunately, helium measurements in literature have ended some years ago, so data on some discharge regimes is unavailable.

Wide-view CXRS system at C-Mod - current layout



- The light is collected by two optical periscopes (red and blue) and transmitted through two fiber bundles to holographic imaging spectrograph.
- Spectrograph is set up to accept the light from up to 45 spatial channels and spectrally disperse them onto the CCD detector, while keeping them spatially separated.

Two Plasma Viewing Arrays

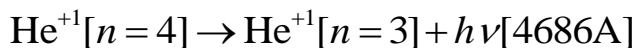
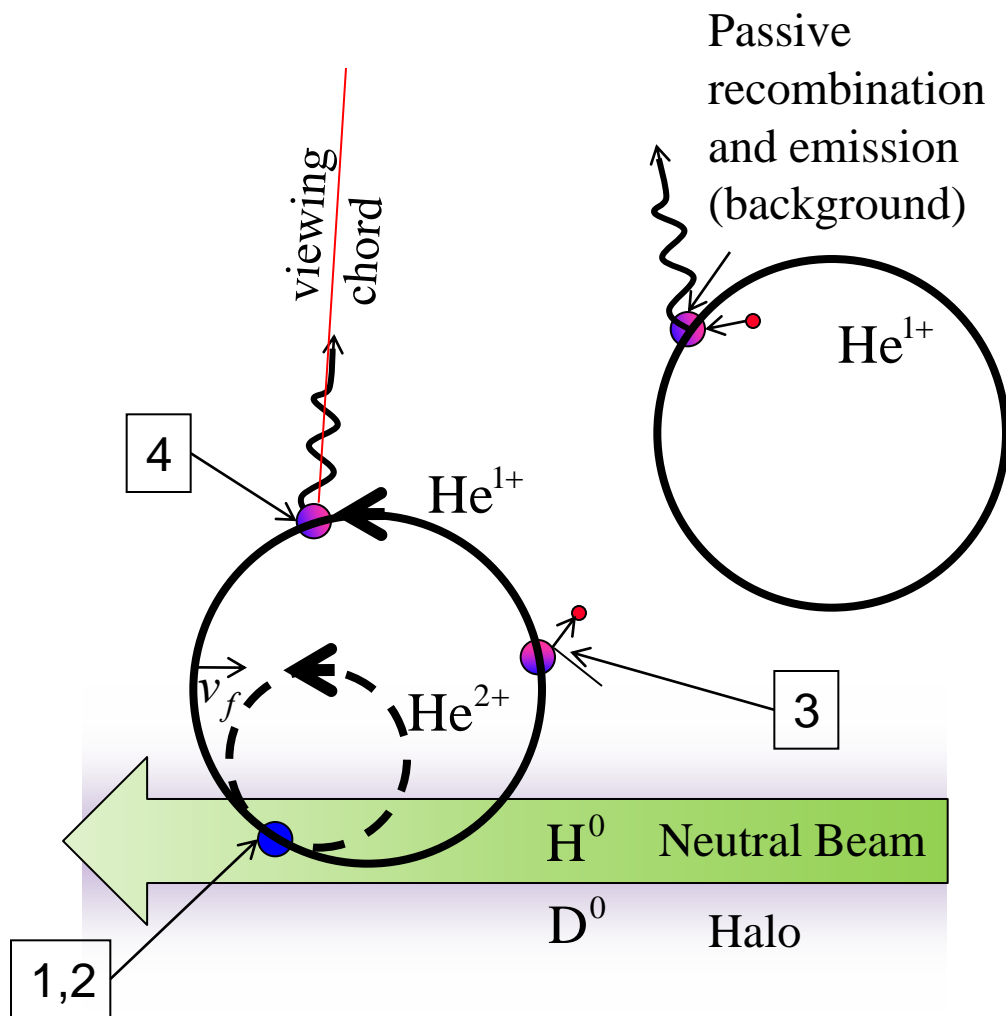


Poloidal coverage: 0.650m to 0.896m ($\rho \approx 0$ to 1)

Toroidal coverage: 0.720m to 0.839m ($\rho \approx 0.29$ to 0.79)

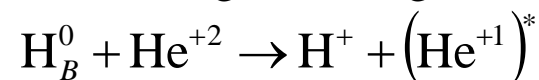
Data from run 1110323 was limited to 15 channels, but new data will use 30 channels

Physics of CXRS

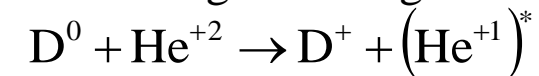


Interactions (partial list):

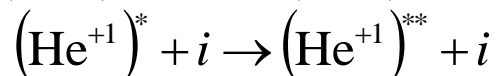
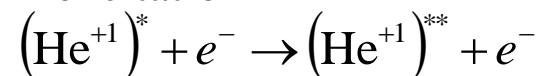
1. DNB charge exchange



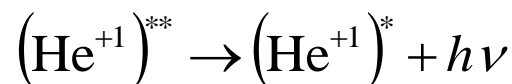
2. Halo charge exchange



3. Collisional excitation/de-excitation



4. Spontaneous emission



$$\lambda = \lambda_0 \left(1 + \frac{v}{c} \cos(\theta) \right)$$

5. Ionization



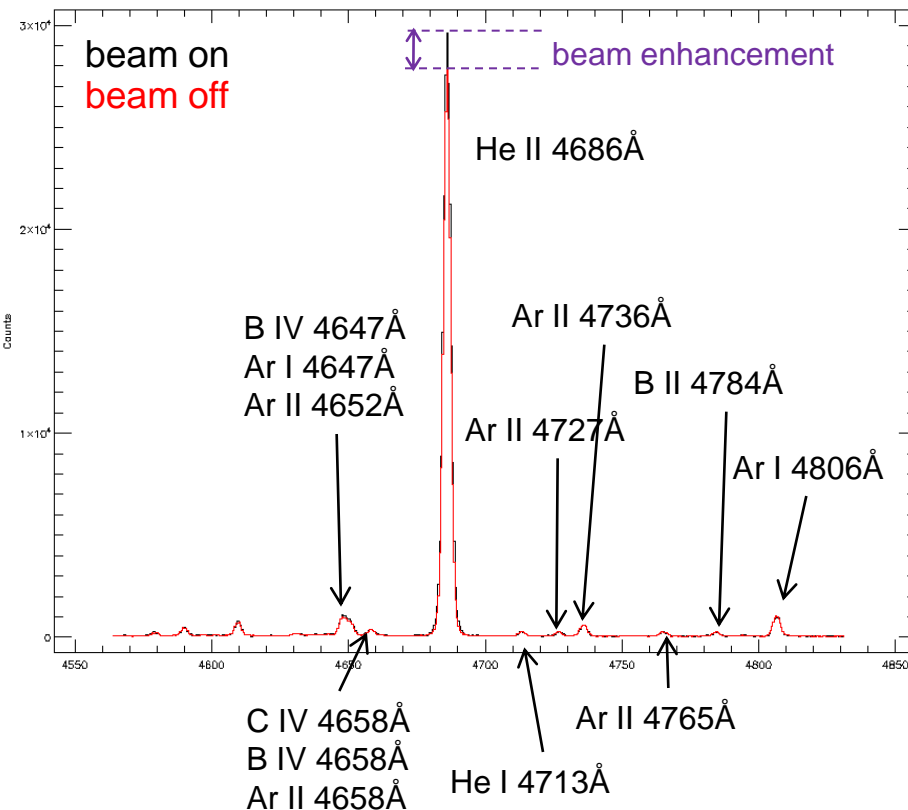
Physics of CXRS

- ◆ In the core of a tokamak plasma, the primary ionization stage for light impurities is fully stripped, which produces no line emission. The technique of CXRS is to observe line emission from partially stripped impurities which briefly exist following charge exchange or recombination.
- ◆ At C-Mod, a 50keV diagnostic neutral beam operating in hydrogen is used as source of active charge exchange. This provides localization of ion measurements and sensitivity in the core.
- ◆ The beam is modulated to allow time-slice subtraction of the background.
- ◆ Helium CXRS is particularly challenging because the cross section for charge exchange with the neutral beam is small and the passive background emission is large.
- ◆ The He^{1+} [n=4 \rightarrow 3] 4686Å transition is used here.

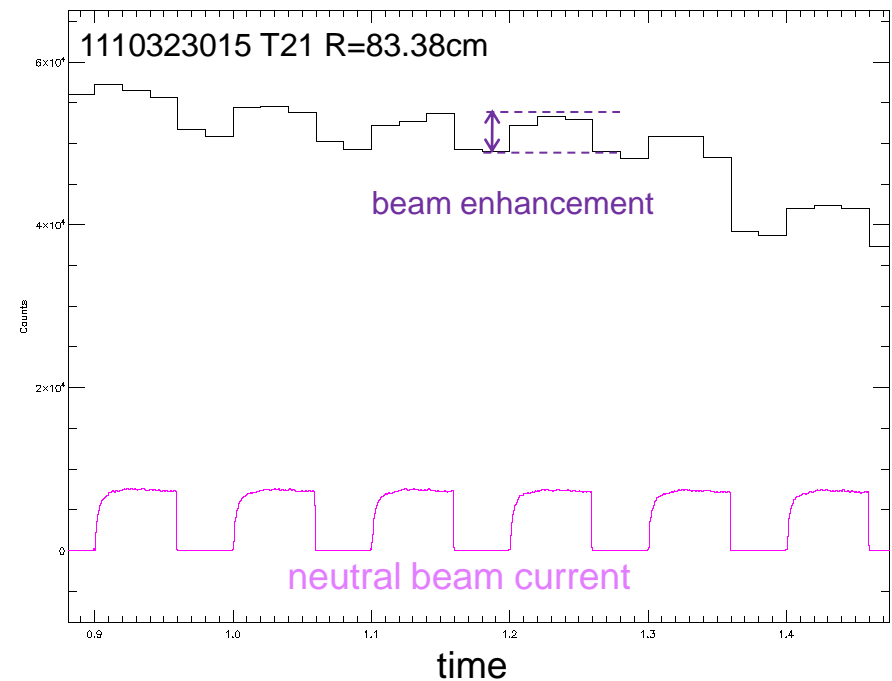
He II 4686Å Spectrum from one channel

- ◆ Beam enhanced signal is obtained by subtracting background signal with beam off which is due to cold edge ions and passive CXRS.
- ◆ Subtraction is imperfect because the background emission is evolving. This is a major source for measurement noise.

Spectral region near He II 4686Å line



Area of He II 4686Å line over time



beam enhancement is visible, but may be swamped by changes in plasma state

Emission

For a general (non-thermal) impurity distribution, the emissivity is:

$$\varepsilon(\lambda)dVd\Omega = \frac{1}{4\pi} \sum_m n_{b,m} \int f(\vec{v}) \sigma \left(\frac{1}{2} m |\vec{v} - \vec{v}_m|^2 \right) \sum_k a_k \delta \left[\lambda - \lambda_k \left(1 + \frac{v \cos \alpha}{c} \right) \right] d^3v$$

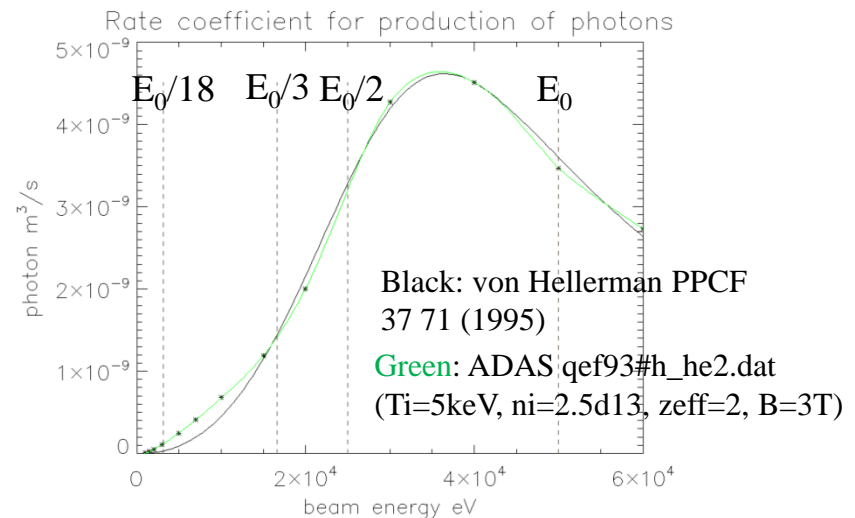
sum over beam energy components ion velocity distribution function effective cross section for charge exchange and emission beam velocity sum over line components angle between ion and viewing chord

When the distribution is approximately thermal, the expression simplifies:

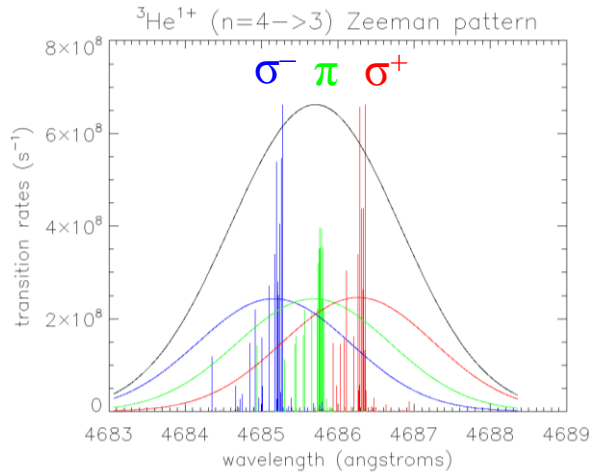
$$\varepsilon(\lambda)dVd\Omega = \frac{1}{4\pi} \sum_m n_{b,m} n_{He} q_{eff} \sum_k a_k \exp \left(- \frac{(\lambda - \lambda_k (1 + \langle v \rangle \cos \alpha / c))^2 m_{He} c^2}{2T \lambda_k^2} \right)$$

The effective rate coefficient, q_{eff} , combines the cross section for charge exchange into various initial energy states with a collisional-radiative model to compute the amount of photon emission. q_{eff} depends on electron density, temperature, magnetic field, and effective Z .

For 4686A, halo emission is negligible.



Helium Line Fitting



4686A He¹⁺ line is split by Zeeman effect

146 transition lines for ³He (n:4→3)

286 transition lines for ⁴He (n:4→3)

Zeeman pattern is obscured by instrument function and Doppler broadening, but is needed for proper width fitting. Pattern is polarized and depends on viewing angle.

Fit spectral data with model function

$$y = a_0 \sum_{i=1}^{146} \exp\left(-\frac{[x - \lambda_i(1 + a_1/c)]}{a_2}\right) + a_3$$

use Levenberg-Marquadt solver “mpfit”

H_k was obtained in multiple ways:

- ❖ bremsstrahlung – calculate throughput using measured continuum level and expected bremsstrahlung
- ❖ beam into gas – calculate from emission from beam fired into vessel filled with neutral helium gas
- ❖ radiometric – backlight with integrating sphere
- ❖ quasineutrality – scale to Thompson Scattering measurement of electron density for helium plasma

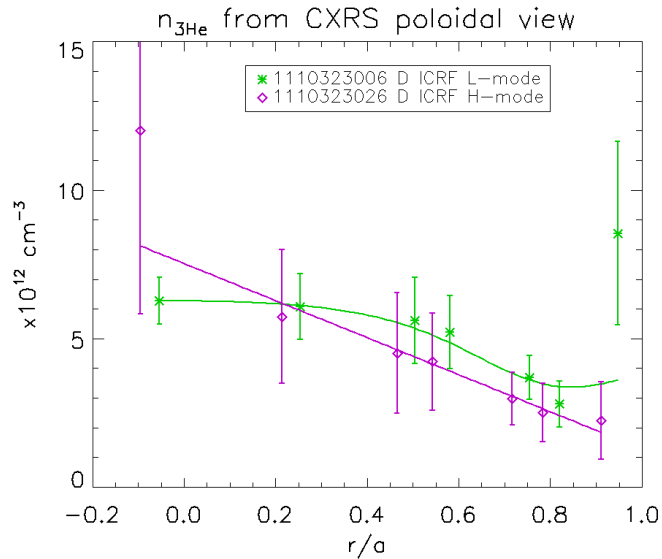
$$\underbrace{n_{He}}_{\text{density}}(\rho_k) = a_0 \underbrace{\sqrt{\pi a_2}}_{\text{calibration factor}} / H_k / \underbrace{\int n_b ds}_{\text{beam density integral}}$$

$$\underbrace{\mathbf{v}_{He}(\rho_k) \cdot \mathbf{s}_k}_{\text{velocity along viewing chord}} = a_1 - \underbrace{Y_k}_{\text{calibration factor}}$$

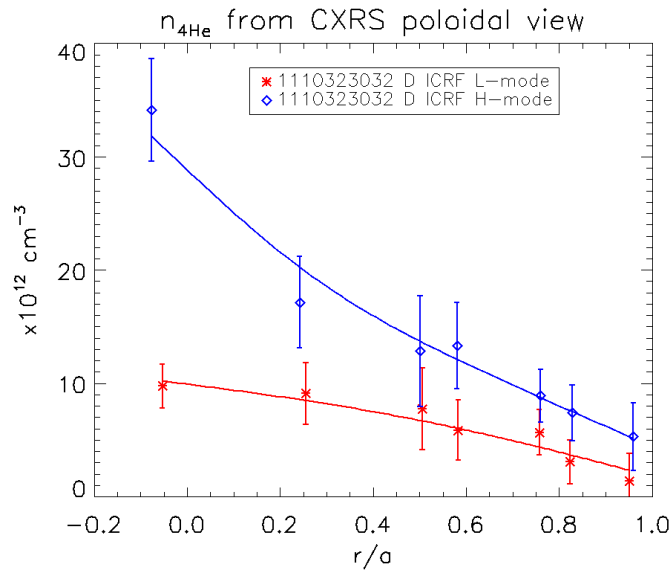
$$\underbrace{T(\rho_k)}_{\text{temperature}} = \left(a_2 - \underbrace{\Delta\lambda_{inst}}_{\text{instrument function}}\right) \frac{m_{3He} c^2}{\lambda_0^2}$$

Helium Profiles

^3He
minority,
D majority



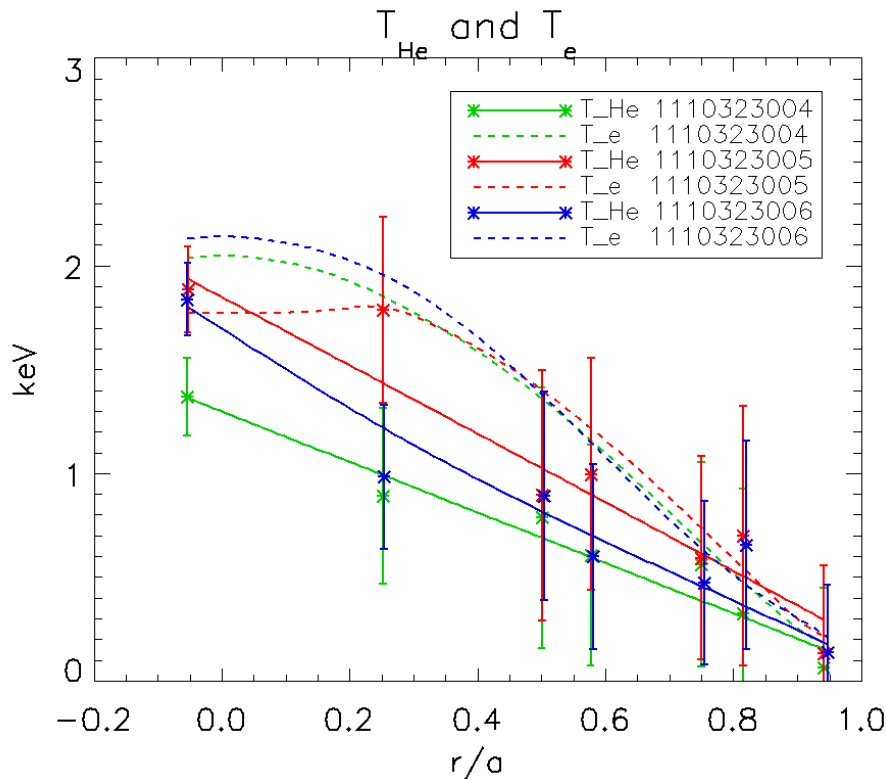
^4He
main ion
plasma



- ◆ During ICRF minority heating experiment with ^3He as the minority species, $n_{^3\text{He}}$ is more strongly peaked in the core in H-mode than in L-mode.
- ◆ This feature is repeated in pure helium plasma discharge.
- ◆ Main ion density is increased during H-mode due to increased particle confinement.

However, data for H-mode discharges is limited to a few shots.

Temperature Profiles

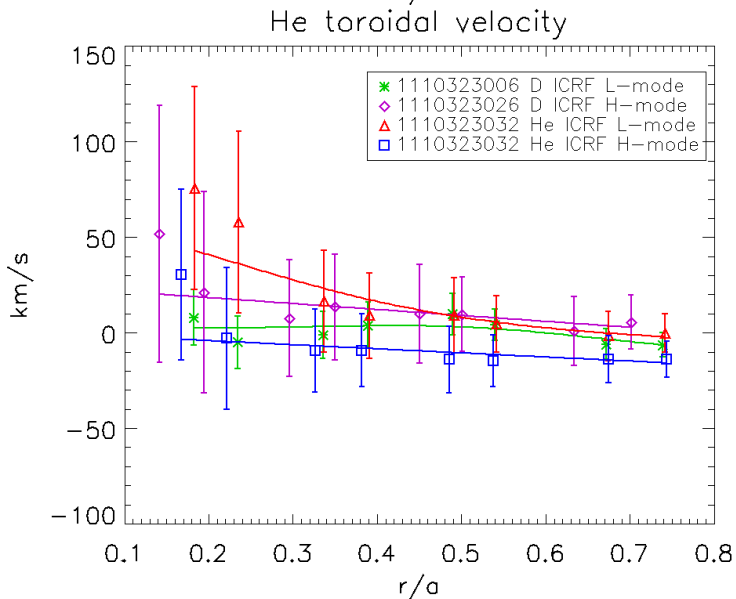
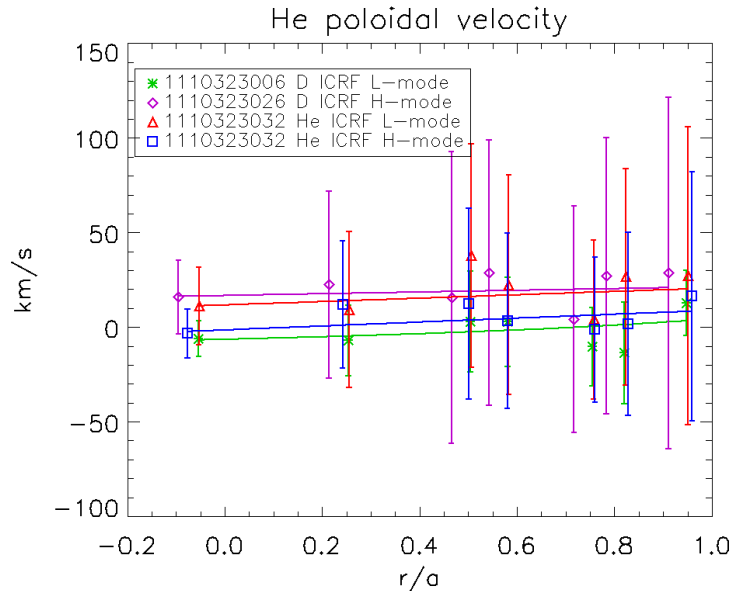


- ◆ Deuterium plasma with helium-3 minority.
- ◆ ICRF mode conversion heating applied
- ◆ In $D(^3\text{He})$ plasma with moderate ^3He concentration ($n_{^3\text{He}}/n_e \sim 10\%$), the waves can be mostly converted to short wavelength slow waves, ICW and IBW, near the mode conversion surface ($D\text{-}^3\text{He}$ hybrid layer) and directly heat electrons and ions.

Mode Conversion Experiment with $D(^3\text{He})$ plasma. Dotted line is electron temperature measured by Thompson Scattering diagnostic. Solid line is He CXRS.

Shot	$n_{^3\text{He}}/n_e$
4	0.05
5	0.07
6	0.23

Velocity profiles



- ◆ Velocity profiles are fitted from CXRS Doppler shifts
- ◆ Calibration of zero velocity taken from fitting beam into helium gas
- ◆ Possibly, there is some poloidal velocity
- ◆ Unfortunately, errors are large, but we have improved throughput for future measurements
- ◆ “Toroidal” velocity is measured at an approximately 40 degree angle from horizontal due to vessel space constraints

Helium Transport

- ◆ Transport in a tokamak is described in terms of neoclassical (or collisional) and anomalous contributions. The anomalous transport is taken to be due to turbulence.
- ◆ Turbulent transport is the dominant impurity transport mechanism in Alcator C-mod; however, we find that neoclassical predictions match the shape of the density profile fairly well.
- ◆ C-mod operate in the banana collisional regime, where bounce frequency exceeds effective collision rate.
- ◆ In drift wave turbulence, correlations between electric potential oscillations and pressure oscillations generate finite gyro-averaged $E \times B$ drifts, leading to radial flux $\Gamma_s = \langle \tilde{n}_s \tilde{v}_{Er} \rangle$
- ◆ Density and temperature gradients and curvature act as sources of free energy for growth of turbulent oscillations.
- ◆ In toroidal geometry, ion temperature gradient (ITG), electron temperature gradient (ETG), and trapped electron modes (TEM) are important contributions to turbulent transport.
- ◆ In ^3He mode conversion experiments, helium concentrations are too high to be treated as tracer particles ($n_{\text{He}} / n_e \sim 0.05 - 0.30$) so helium plays an active role in the drift wave analysis.

Transport Parameterization

- ◆ A standard empirical parameterization is to split the radial transport into a pinch (convection) term and a diffusion term

$$\Gamma_s = -D_s \frac{dn_s}{dr} + v_s n_s$$

- ◆ This parameterization works well for models with linear dependence on density such as neoclassical transport, and allows for direct comparison to experiment. For nonlinear models, an approximate v and D can be found.
- ◆ We assume steady state condition, $\Gamma_s = 0$, during flat top of experimental discharge. Under this condition, v/D is equal to the logarithmic density gradient which can be measured.

$$\frac{v_s}{D_s} = \frac{1}{n_s} \frac{dn_s}{dr} \equiv -L_{n_s}^{-1}$$

$$R \frac{v_s}{D_s} = R \frac{1}{n_s} \frac{dn_s}{dr} \equiv -RL_{n_s}^{-1}$$

- ◆ The neoclassical case has been simulated using NCLASS*

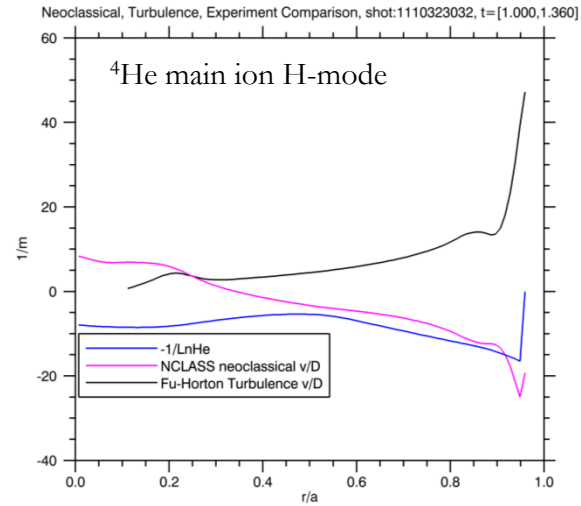
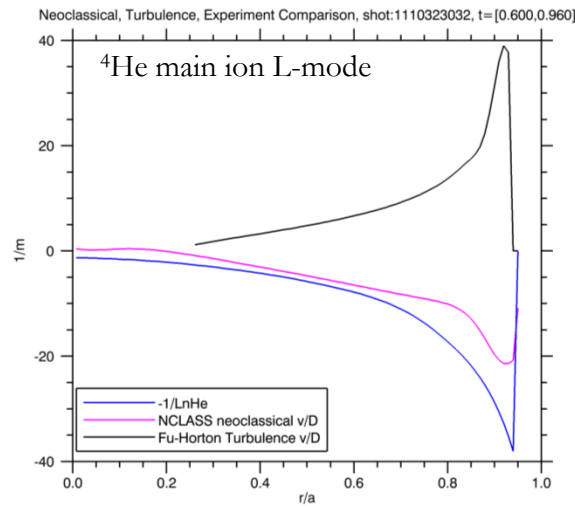
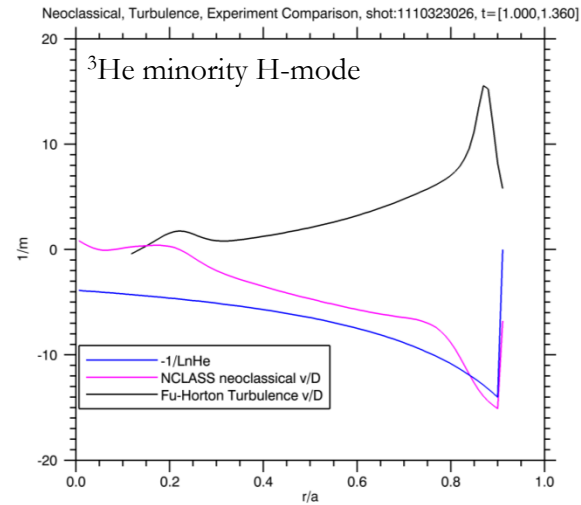
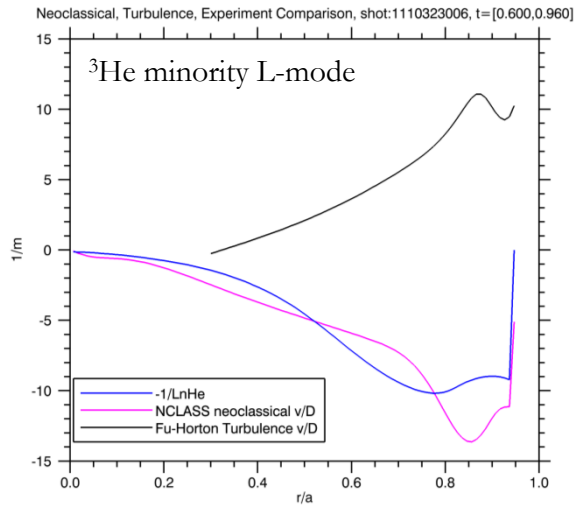
Turbulent Transport

- ◆ See Fu “Turbulent impurity transport modeling for C-Mod” Poster P12 Wed Apr 11 at this conference.
- ◆ Quasilinear particle fluxes Γ_s are calculated from out of phase components of $\delta n_D / \delta \phi$, and $\delta n_{He} / \delta \phi$ and $\delta n_e / \delta \phi$ fluctuations for each k vector. The turbulence level is determined from the growth rate spectrum the determinant of the 4X4 matrix =0.

$$\begin{bmatrix} 1 & Z & -1 & -f_p \\ -i\omega & 0 & 0 & i\omega_{*i} - i(\omega + i\mu_i k_{\perp}^2) k_{\perp}^2 \rho_{s,i}^2 \\ 0 & -i\omega & 0 & i\omega_{*z} - i(\omega + i\mu_z k_{\perp}^2) k_{\perp}^2 \rho_{s,z}^2 \\ 0 & 0 & -i\omega + i\omega_{De} + \nu_{eff} & i\omega_{*e} f_t + i\omega_{De} f_t \end{bmatrix} \begin{bmatrix} \frac{\delta n_i}{n_e} \\ \frac{\delta n_z}{n_e} \\ \frac{\delta n_e}{n_e} \\ \frac{e\phi}{T_e} \end{bmatrix} = \begin{bmatrix} 0 \\ 0 \\ 0 \\ 0 \end{bmatrix}$$

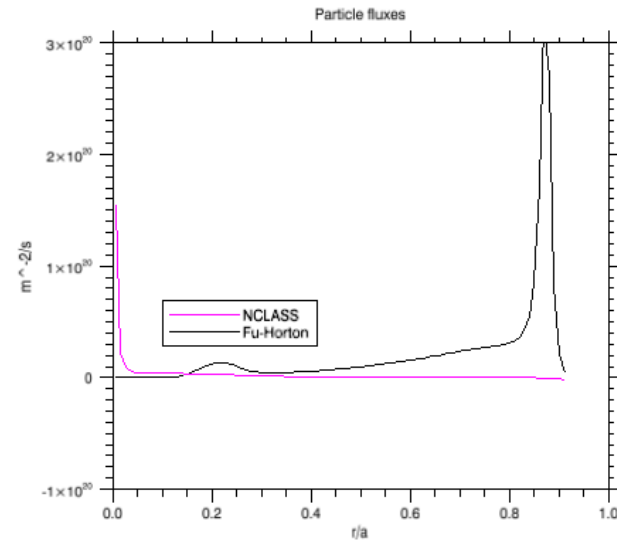
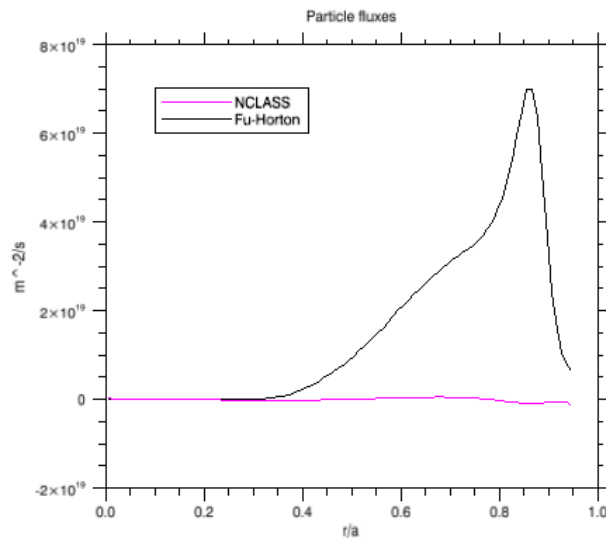
- ◆ Impurity and main ion are treated symmetrically, so we are able to treat cases where helium concentration is comparable to main ion concentration or helium is the main ion.

Transport Simulation



Transport Simulation 2

- ◆ The neoclassical code NCLASS gives similar results to experimental helium inverse scale length.
- ◆ NCLASS predicts a hollower profile in the core in H-mode than we observe.
- ◆ Fu-Horton model produces an outward convective velocity, giving a v/D of opposite sign.



- ◆ Turbulent flux is larger than neoclassical, although ultimately, the flux must cancel with additional terms and precise measurement in steady state plasma.

Parametric sensitivities

- ◆ Experimental parametric sensitivities may guide theoretical work and show the dominant contributions.

- ◆ neoclassical:

$$\Gamma_z \propto -v_z \left\{ \frac{c_1}{Z_i n_i} \frac{\partial n_i}{\partial r} - \frac{c_2}{Z_z n_z} \frac{\partial n_z}{\partial r} + \frac{c_3}{T_z} \frac{\partial T_z}{\partial r} \right\}$$

- ◆ TEM:

- Growth rate decreasing with v_{*e}
- inward thermodiffusion term, outward parallel compression term

- ◆ ITG:

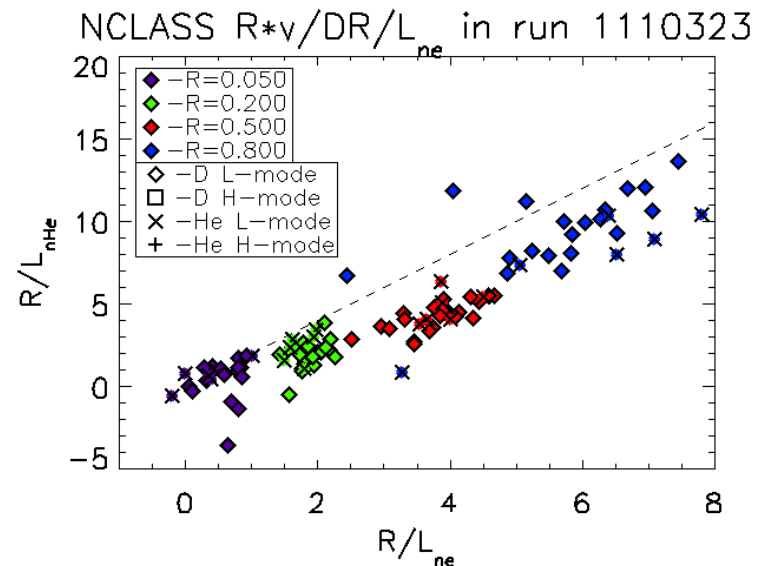
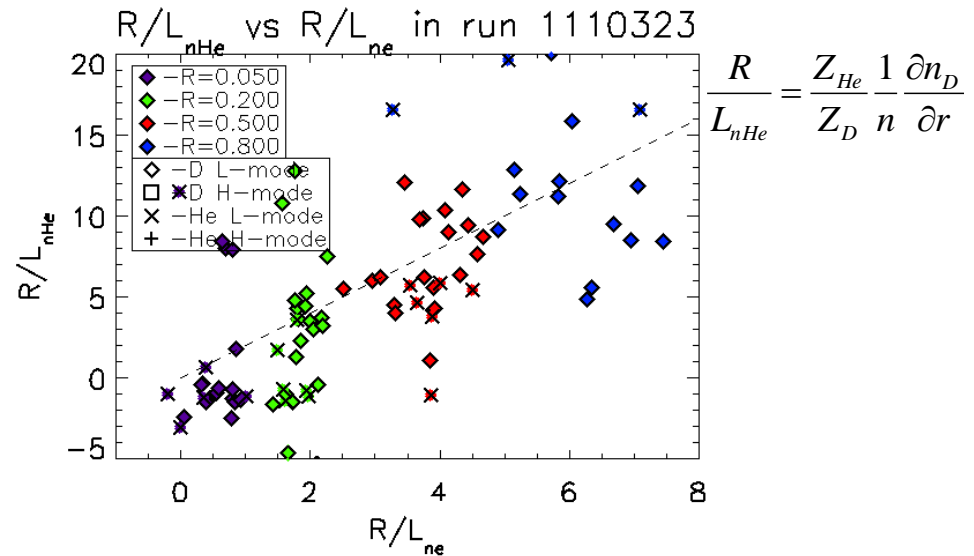
- destabilized by $\eta_s = \frac{d \ln T_s}{d \ln n_s} = \frac{1/L_{Ts}}{1/L_{ns}} > \frac{2}{3}$

- outward thermodiffusion term, inward parallel compression term

- ◆ See also, Rowan “Transport of light, trace impurities in Alcator C-Mod” Poster P16 Tue Apr 10 at this conference.

R/L_{nHe} vs R/L_{ne}

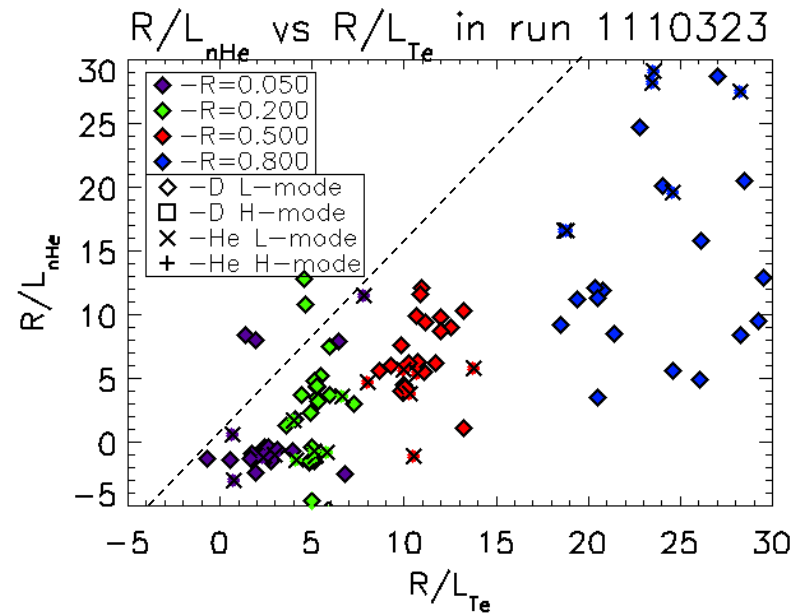
- ◆ Experimental values from 24 shots are plotted
- ◆ He density from He CXRS poloidal view
- ◆ Electron density from Thompson Scattering diagnostic
- ◆ This is compared to neoclassical calculation of v/D versus experimental electron logarithmic density gradient.
- ◆ Dotted line is a neoclassical scaling, neglecting thermodiffusion terms. Lower right simulation points have thermodiffusion included.



R/L_{nHe} vs R/L_{Te}

- ◆ He density from He CXRS poloidal view
- ◆ Electron temperature from Thompson Scattering diagnostic
- ◆ Below dotted line is ITG unstable region if T_e used as a proxy for T_{He}

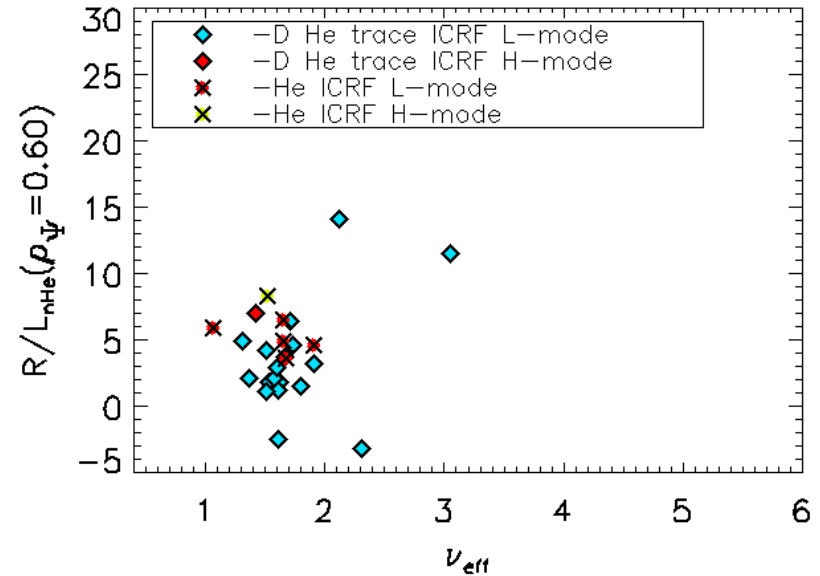
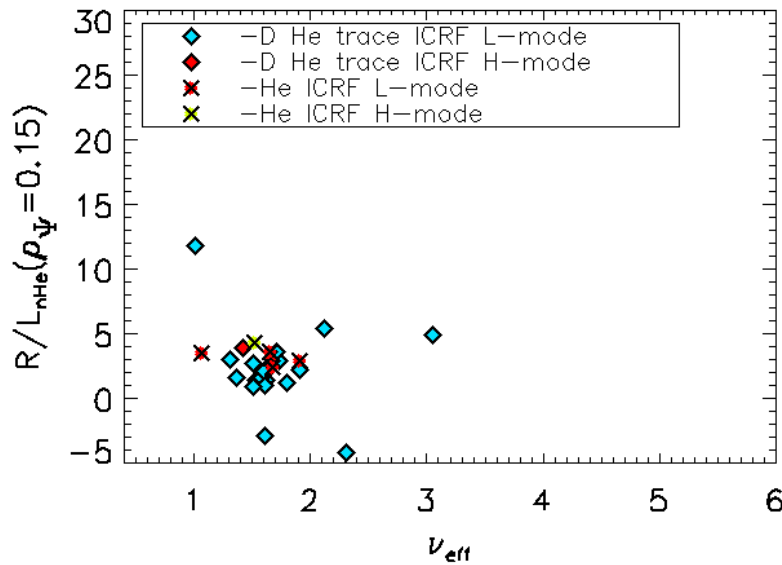
$$\frac{R/L_{Te}}{R/L_{nHe}} = \frac{2}{3}$$



L_{nHe} vs ν_{eff}

$$\nu_{eff} = 0.1 \frac{Z_{eff} \langle n_e \rangle R}{\langle T_e \rangle^2} \sim \frac{\nu_{ei}}{\omega_{De}}$$

Expresses strength of collisional processes to characteristic turbulent processes



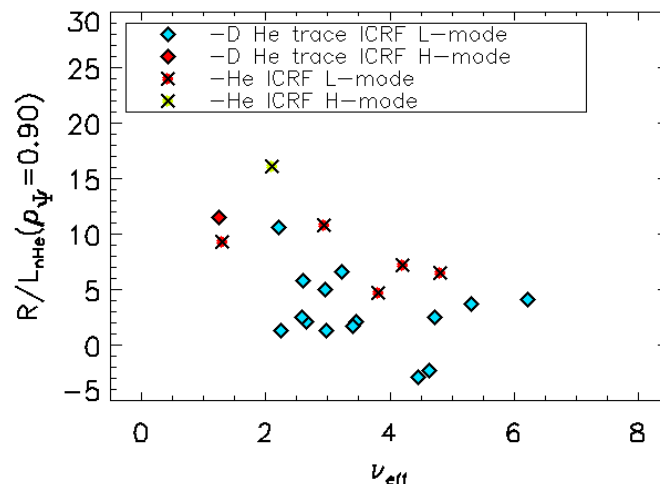
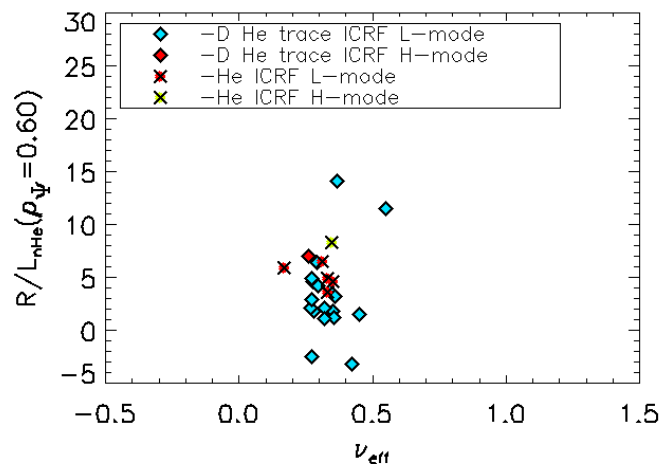
Perhaps insufficient data in diverse operating scenarios to make a conclusion
 R/L_{nHe} generally is close to neoclassical prediction

L_{nHe} VS v_{*e}

$$v_{*e} = \sqrt{2} \left(\frac{v_e q R}{\varepsilon^{3/2} v_e} \right)$$

Expresses ratio of collision frequency to bounce time

$v_{*e} < \sim 1$ indicates banana regime and destabilization of trapped electron modes



In core, little collisionality variation is available and no dependence is visible.
Near edge, a wider distribution of collisionality is available.
There is a steepening of the density profile due to increasing diffusion.
TEM is not expected to play a role at high v_{*e}